SINTEF
PROCEEDINGS
2

Proceedings of the 12th International Conference on Computational Fluid Dynamics in the Oil & Gas, Metallurgical and Process Industries

Progress in Applied CFD – CFD2017

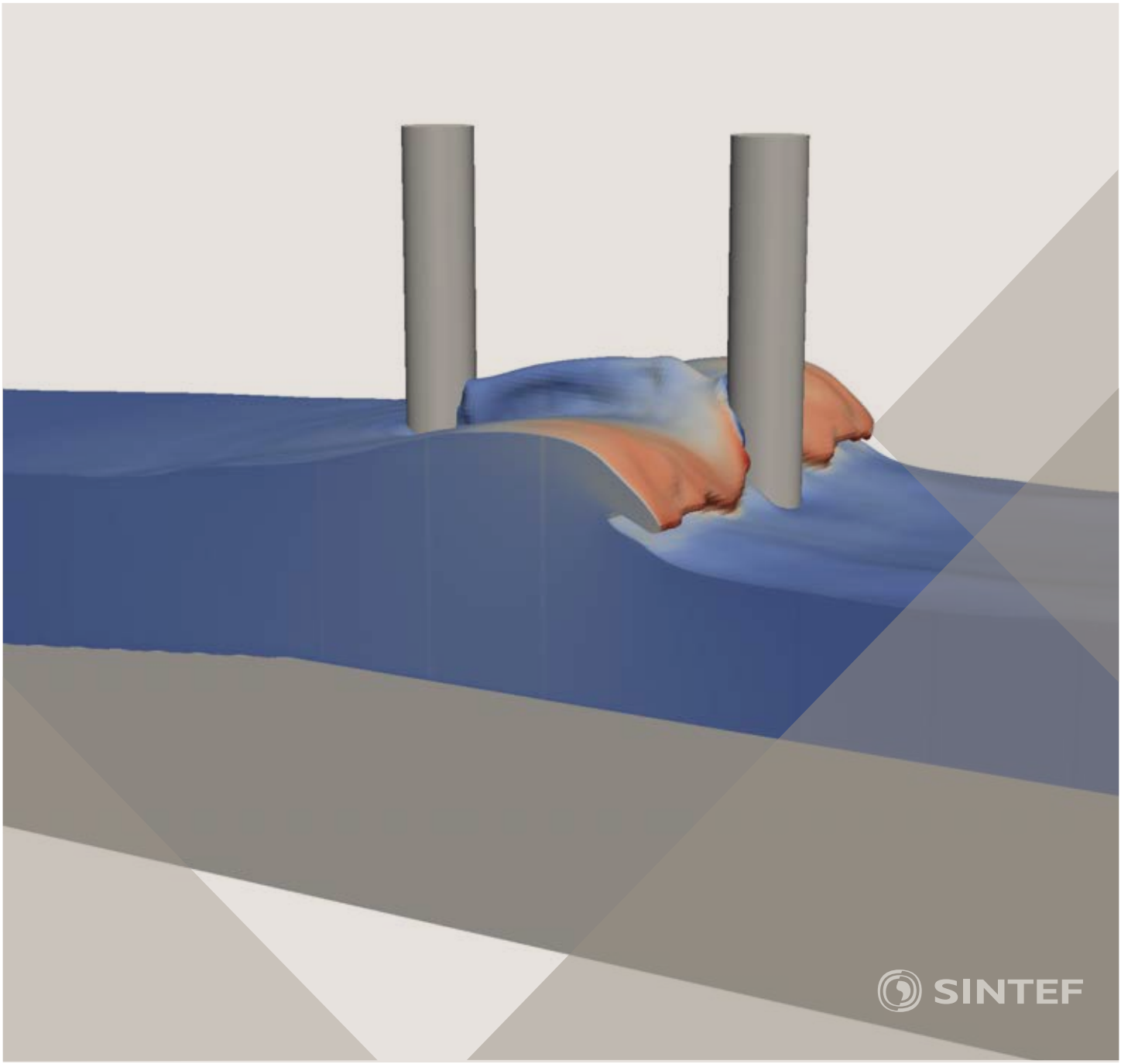

SINTEF Proceedings

Editors:
Jan Erik Olsen and Stein Tore Johansen

Progress in Applied CFD – CFD2017

Proceedings of the 12th International Conference on Computational Fluid Dynamics in the Oil & Gas, Metallurgical and Process Industries

SINTEF Academic Press

SINTEF Proceedings no 2
Editors: Jan Erik Olsen and Stein Tore Johansen
Progress in Applied CFD – CFD2017
Selected papers from 10th International Conference on Computational Fluid Dynamics in the Oil & Gas, Metallurgical and Process Industries

Key words:
CFD, Flow, Modelling

Cover, illustration: Arun Kamath

ISSN 2387-4295 (online)
ISBN 978-82-536-1544-8 (pdf)

SINTEF Academic Press
Address: Forskningsveien 3 B
PO Box 124 Blindern
N-0314 OSLO
Tel: +47 73 59 30 00
Fax: +47 22 96 55 08

www.sintef.no/byggforsk
www.sintefbok.no

SINTEF Proceedings
SINTEF Proceedings is a serial publication for peer-reviewed conference proceedings on a variety of scientific topics.
The processes of peer-reviewing of papers published in SINTEF Proceedings are administered by the conference organizers and proceedings editors. Detailed procedures will vary according to custom and practice in each scientific community.

PREFACE

This book contains all manuscripts approved by the reviewers and the organizing committee of the 12th International Conference on Computational Fluid Dynamics in the Oil & Gas, Metallurgical and Process Industries. The conference was hosted by SINTEF in Trondheim in May/June 2017 and is also known as CFD2017 for short. The conference series was initiated by CSIRO and Phil Schwarz in 1997. So far the conference has been alternating between CSIRO in Melbourne and SINTEF in Trondheim. The conferences focuses on the application of CFD in the oil and gas industries, metal production, mineral processing, power generation, chemicals and other process industries. In addition pragmatic modelling concepts and bio-mechanical applications have become an important part of the conference. The papers in this book demonstrate the current progress in applied CFD.

The conference papers undergo a review process involving two experts. Only papers accepted by the reviewers are included in the proceedings. 108 contributions were presented at the conference together with six keynote presentations. A majority of these contributions are presented by their manuscript in this collection (a few were granted to present without an accompanying manuscript).

The organizing committee would like to thank everyone who has helped with review of manuscripts, all those who helped to promote the conference and all authors who have submitted scientific contributions. We are also grateful for the support from the conference sponsors: ANSYS, SFI Metal Production and NanoSim.

Stein Tore Johansen & Jan Erik Olsen

Organizing committee:

Conference chairman: Prof. Stein Tore Johansen
Conference coordinator: Dr. Jan Erik Olsen
Dr. Bernhard Müller
Dr.Sigrid Karstad Dahl
Dr.Shahriar Amini
Dr.Ernst Meese
Dr.Josip Zoric
Dr.Jannike Solsvik
Dr.Peter Witt

Scientific committee:

Stein Tore Johansen, SINTEF/NTNU
Bernhard Müller, NTNU
Phil Schwarz, CSIRO
Akio Tomiyama, Kobe University
Hans Kuipers, Eindhoven University of Technology
Jinghai Li, Chinese Academy of Science
Markus Braun, Ansys
Simon Lo, CD-adapco
Patrick Segers, Universiteit Gent
Jiyuan Tu, RMIT
Jos Derksen, University of Aberdeen
Dmitry Eskin, Schlumberger-Doll Research
Pär Jönsson, KTH
Stefan Pirker, Johannes Kepler University
Josip Zoric, SINTEF

CONTENTS

12th International Conference on CFD in Oil & Gas, Metallurgical and Process Industries
SINTEF, Trondheim, NORWAY
May 30th - June 1st, 2017

FROM LINEAR TO NONLINEAR: TRANSIENT GROWTH IN CONFINED MAGNETOHYDRODYNAMIC FLOWS

Oliver G. W. CASSELLS[1*], **Tony VO**[1†], **Alban POTHÉRAT**[2‡], **Gregory J. SHEARD**[1§]

[1]Department of Mechanical and Aerospace Engineering, Monash University, Victoria 3800, Australia

[2]Applied Mathematics Research Centre, Coventry University, Coventry, CV15FB, United Kingdom

[*] E-mail: oliver.cassells@monash.edu
[†] E-mail: tony.vo@monash.edu
[‡] E-mail: aa4111@coventry.ac.uk
[§] E-mail: greg.sheard@monash.edu

ABSTRACT

The underlying flow mechanisms for the destabilisation of an electrically conducting fluid under the influence of a transverse magnetic field in a square duct are investigated. Such flows are applicable to metallurgical processes where magnetic fields are used to dampen disturbances to increase homogeneity in material production, in addition to cooling blankets of nuclear fusion reactors, where flow disturbances can aid in improving convective heat transfer. A preliminary investigation into optimal linear growths at Hartmann numbers $10 \leq Ha \leq 1000$ and Reynolds number $Re = 5000$ identifies two regimes for the scaling of optimal linear growths; when perturbation structures are dominated by three-dimensional variation in the vertical side-wall boundary layers, and for when quasi-two-dimensional (Q2D) disturbances are prevalent. Through comparison with existing literature, the Q2D model of Sommeria & Moreau (1982) is shown to be an excellent predictor of fundamental growth mechanisms for $Ha > 150$. A two-step method incorporating the seeding of an unperturbed base flow with optimal linear perturbations in a high magnetic field strength regime shows that no increase in energy amplification can be achieved via initial seeding energies in the range $10^{-6} \leq E_p \leq 10^{-2}$. The dominant dissipative mechanisms for these different seeding energies are also analysed, where it is shown that strong magnetic damping does not always necessitate the smoothing of the velocity field towards pure anisotropy, which has potentially useful applications for aiding convective heat transfer in magnetically damped flows.

Keywords: CFD, transient linear growth, magnetohydrodynamics, liquid metal, fusion reactor, metallurgy.

NOMENCLATURE

Greek Symbols

δ	Boundary layer thickness
ϵ	Viscous dissipation
μ	Magnetic dissipation
ν	Kinematic viscosity
Ω	Spatial domain
ϕ	Electric scalar potential
ρ	Mass density
σ	Electrical conductivity
τ	Time period
ξ	Shape function L_i spatial coordinate

Latin Symbols

$\mathcal{A}$	State-transition operator
a	Duct width
$\boldsymbol{B_0}$	Magnetic field vector
B_0	Magnetic field magnitude
C_d	Viscous drag coefficient
E	Kinetic energy
G	Perturbation energy amplification
$\mathcal{G}$	Anisotropy coefficient
Ha	Hartmann number
$\boldsymbol{j}$	Electric current density vector
$\boldsymbol{k}$	Wavenumber vector
k	Streamwise wavenumber.
L	Linear time evolution operator.
L_i	Lagrangian polynomial shape function.
L_z	Periodicity duct length
$\mathcal{L}^2$	Vector space
m	Fourier mode
N_p	Shape funtion polynomial order
p	Pressure
Re	Reynolds number
Re_m	Magnetic Reynolds number
t	Time
U_0	Peak base flow streamwise velocity
u	x-velocity component of $\boldsymbol{V}$
$\boldsymbol{V}$	Velocity vector
v	y-velocity component of $\boldsymbol{V}$
w	z-velocity component of $\boldsymbol{V}$
x	Cartesian coordinate (spanwise direction)
y	Cartesian coordinate (spanwise direction)
z	Cartesian coordinate (streamwise direction)

Sub/superscripts

g	Nodal index
Ha	Hartmann layer
i	Nodal index
m	Fourier coefficient
max	Global maximum
n	Non-linear solution
opt	Optimal value at global maximum
p	Perturbation field
Sh	Shercliff layer
0	Base flow
$\hat{}$	Fourier transform
$\prime$	Linear perturbation
$*$	Adjoint

INTRODUCTION

Electrically conducting fluids under the influence of strong magnetic fields come under the class of magnetohydrodynamic (MHD) flows. Understanding the stability mechanisms of such flows has potentially significant implications to metallurgical processes, and more pertinently the viability of clean energy sources, such as magnetic confinement fusion reactors. For the latter, the strong transverse magnetic fields that exist to contain the plasma have a strong damping effect on the flow differentials in the adjacent liquid metal cooling blankets. In these flows, motion-derived electric currents interact with an externally applied magnetic field to induce electro-magnetic forces known as Lorentz forces (Hunt and Stewartson, 1965). The Lorentz force acts to suppress velocity differentials in perpendicular planes, while flow structures also become elongated and aligned with the external magnetic field vector (Sommeria and Moreau, 1982; Sommeria, 1988). Furthermore, boundary layers develop along walls aligned with the magnetic field (called Shercliff layers) and orthogonal to it (Hartmann layers). Both become thinner at higher magnetic fields, as their thicknesses respectively scale as $\delta_{Sh} = O(Ha^{-1/2})$ and $\delta_{Ha} = O(Ha^{-1})$. Here, Ha is the Hartmann number describing the ratio of electromagnetic to viscous forces in the flow and is a function of the geometry and material properties of the fluid.

A resulting effect of these flow modulations is inefficient convective heat transport; a detriment to the thermal performance in maintaining safe operating temperatures of the reactor, and in the heat exchange process used in the production of electrical energy. To overcome these issues, several works have been conducted with the aim of mechanically enhancing the convective heat transfer performance (Cassells *et al.*, 2016; Hamid *et al.*, 2016). While these methods certainly hold an important place in furthering our current understanding, as well as our ability to meet the viability constraints of fusion reactors, they are not always practicable. Thus, a further understanding of the underlying instability mechanisms which can aid in convection across a broader range of operational parameters is needed.

An issue with respect to studying the stability of MHD flows in the limit of strong magnetic fields is the discrepancy between the critical regime parameters predicted through the growth of exponentially growing perturbations and that observed in experiments. For example, it has been shown that the Hartmann boundary layers become linearly unstable for $Re/Ha \geq 48311$, whereas experimental observations show transition occurring for $Re/Ha \geq 380$ (Takashima, 1996; Moresco and Alboussiere, 2004; Krasnov *et al.*, 2004, 2010). One explanation is that the non-normality of the Orr–Sommerfeld modes can create transient amplifications leading to a subcritical instability. In other words, the linearisation around a base state may predict asymptotically decaying eigenvalues, yet, interactions between suboptimal modes could result in sufficient non-linear transient amplifications to render the base flow unstable (Náraigh, 2015). The initial conditions that undergo the maximum growth in kinetic energy are commonly referred to as the optimal perturbations or modes.

The three-dimensional nature of MHD flows and the reduction in boundary layer thickness (relative to hydrodynamic flows) means that numerically such analysis comes at a large computational cost. Quasi-two-dimensional (Q2D) numerical models for approximating these flows at high magnetic field strengths are often utilised by assuming the flow outside of laminar Hartmann boundary layers are predominantly two dimensional. First developed by Sommeria and Moreau (1982) (hereafter SM82), this model has proved promising from a kinematic standpoint for when both the Hartmann number and the interaction parameter, defined as $N = Ha^2/Re$, are much greater than unity, where Re is the Reynolds number representing the ratio of inertial to viscous forces in the flow (Sommeria and Moreau, 1982; Pothérat *et al.*, 2000; Hamid *et al.*, 2015; Cassells *et al.*, 2016).

Pothérat (2007) studied the effects of the Shercliff layers on the stability of confined MHD flows using the SM82 model. In this framework, the three-dimensional component of the wavenumber and MHD equivalent Orr–Sommerfeld modes was assumed zero, an assumption expected to become valid when $Ha > 200$. It was further assumed that only the MHD equivalent of the Orr–Sommerfeld modes were available to contribute to non-modal growths. However, the validity of these Q2D approximations on resolving the all-important stability characteristics in three-dimensional MHD flows has been the focus of little to no empirical research. To the best of the authors knowledge, the only methodologically comparable research to that presented in the present work is by Krasnov *et al.* (2010), who employed 3D transient growth analysis to show a scaling of global dominant modes following a $Ha^{-3/2}$ relation in the limited range of $10 \leq Ha \leq 50$ for $Re = 5000$ in square ducts.

The presence and structure of these optimal modes have been shown to form a fundamental part in the processes leading to flow destabilisation and subsequently the transition of fully turbulent flows (Boeck *et al.*, 2008). From an industrial standpoint, effective flow control strategies, such as periodic suppression and/or excitation of electro-magnetic fields, can be implemented to promote or discourage flow destabilisation by utilising the knowledge of the modal and spatial characteristics of these linear growth mechanisms. Potential end uses being the destabilisation of liquid metal cooling blankets to aid convective heat transfer coefficients in nuclear fusion reactors, or the promotion of flow stability to aid in homogeneity of material production in metallurgical applications (Smolentsev *et al.*, 2012).

Motivated by an investigation into the stability of Hartmann layers by Krasnov *et al.* (2004), a two-step method incorporating the seeding of a basic flow in a three-dimensional MHD duct with the optimal disturbance modes will also be investigated in the present work. For Hartmann flows, this method has shown a strong correlation in relation to the types of flow structures which appear during transition and onset of turbulence in full-3D-DNS seeded with small-amplitude random noise and experimental works with varying surface roughness (Krasnov *et al.*, 2004; Moresco and Alboussiere, 2004).

To date, it is not properly understood if Q2D models are accurate predictors of the dominant disturbance mechanisms towards high magnetic field strengths, nor is there an extensive body of work on the physical structures which develop through their transition to a Q2D-dominated state. Therefore, the present work aims to address this gap in knowledge by elucidating the processes for when and how specific linear transient amplifications present over a wide range of Ha, and the processes through which the 3D states at low magnetic field strengths give way to anisotropic 2D structures at higher field strengths. Furthermore, as the energetic response of seeding fully confined 3D MHD flows with opti-

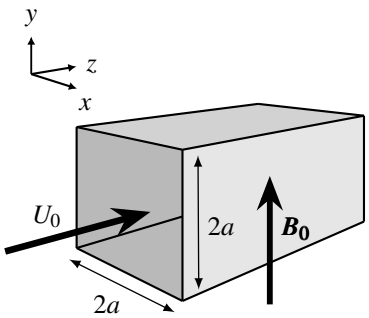

Figure 1: Schematic depicting the flow configuration and parameters pertaining to this investigation.

mal perturbation modes has not been investigated, and poses promising potential applications, it is therefore an additional aim of the present work to extend this to the confined MHD case incorporating the sidewall Shercliff layers. The energetic response for high Ha, in addition to a quantification of the dominant dissipation mechanisms affecting the evolution of kinetic energy and the formation of flow structures will be also investigated.

MODEL DESCRIPTION

Problem Definition and Mathematical Formulation

A fluid with electrical conductivity σ, kinematic viscosity ν and density ρ, flows through a square duct with cross-sectional width $2a$. The electrically insulated vertical and horizontal duct walls are respectively located at $x = \pm a$ and $y = \pm a$. A constant external homogeneous magnetic field $\boldsymbol{B_0} = B_0\boldsymbol{e}$ is imposed on the flow tangential to the vertical sidewalls such that the unit vector $\boldsymbol{e} \equiv \langle e_x, e_y, e_z\rangle = \langle 0,1,0\rangle$ (see figure 1). The flow is driven by a constant pressure gradient ∇p with no-slip conditions applied on all solid boundaries. The MHD equations are written in the quasi-static, low-magnetic number approximation. In this approximation, the magnetic field generated by the motion-induced currents of the conducting fluid in comparison to the externally applied field B_0 are small. Hence, the agglomerated magnetic field remains of nearly equal magnitude to B_0. This approximation is valid for target applications and in laboratory experiments of moderate intensity and size (typically liquid metals flowing under $1m/s$ in a domain smaller than $1m$)(Krasnov *et al.*, 2010; Smolentsev *et al.*, 2010). Non-dimensionalisation of the governing equations is achieved by taking the proper scales for length a, pressure ρU_0^2, where U_0 is the peak inlet velocity, time a/U_0, magnetic field B_0 and lastly, for the electric potential aU_0B_0. It follows that the dimensionless quasi-static momentum and continuity equations can be written as

$$\frac{\partial \boldsymbol{V}}{\partial t} + (\boldsymbol{V}\cdot\boldsymbol{\nabla})\boldsymbol{V} = -\boldsymbol{\nabla}p + \frac{1}{Re}\nabla^2\boldsymbol{V} + \frac{Ha^2}{Re}(\boldsymbol{j}\times\boldsymbol{B_0}), \quad (1)$$

$$\boldsymbol{\nabla}\cdot\boldsymbol{V} = 0, \quad (2)$$

where $\boldsymbol{V}(x,y,z,t) = \langle u,v,w\rangle$ and $\boldsymbol{j} = -\boldsymbol{\nabla}\phi + \boldsymbol{V}\times\boldsymbol{B_0}$ are the velocity and electric current density vectors, respectively. Here ϕ is the electric scalar potential. The dimensionless groups Re and Ha are respectively the Reynolds number, $Re \equiv U_0 a/\nu$, representing the ratio of inertial to viscous forces in the flow, and the Hartmann number, $Ha \equiv aB_0\sqrt{\sigma/\rho\nu}$, representing the ratio of electromagnetic to the viscous forces in the flow. In the present work, Hartmann numbers between $10 \leq Ha \leq 1000$ are investigated which significantly extends the range covered by Krasnov *et al.* (2010). The aim being to bridge the gap between 3D and Q2D models for transient growth analysis of optimal linear amplifications. Here a fixed Reynolds number of $Re = 5000$ is used both for comparison reasons with existing literature, but also as it is below the exponential instability limit found for hydrodynamic Poiseuille flows.

Transient growth analysis

The transient growth of linear three-dimensional infinitesimal perturbations of the form

$$[\boldsymbol{V}_p, \phi_p, p_p](x,y,z,t) = \left(u', v', w', \phi', p'\right), \quad (3)$$

to a streamwise independent two-dimensional steady-state base flow

$$[\boldsymbol{V}_0, \phi_0, p_0] = (u(x,y), v(x,y), w(x,y), \phi(x,y), p(z)), \quad (4)$$

is conducted by tracking their energy amplification over a finite time interval τ. The flow solution then takes the general form

$$[\boldsymbol{V}, \phi, p] = (\boldsymbol{V}_0, \phi_0, p_0) + (\boldsymbol{V}_p, \phi_p, p_p), \quad (5)$$

with the perturbations being considered through the form of decoupled normal Fourier modes

$$[\boldsymbol{V}_p, \phi_p, p_p] = \left(\hat{u}, \hat{v}, \hat{w}, \hat{\phi}, \hat{P}\right)(x,y,t)\cdot e^{ikz}, \quad (6)$$

where k is a streamwise wavenumber. For brevity, the full system of linearised equations describing the evolution of these perturbed flows is not given. The reader may refer to Krasnov *et al.* (2010) for a form consistent with this work.
The growth in perturbation kinetic energy over a given time interval $t = \tau$ can be written as a ratio of volume integrals over domain Ω of the standard $\mathcal{L}^2$ space inner products of $\boldsymbol{V}_p(t)$ at $t = \tau$ over the initial state at $t = 0$

$$G(\tau) = \frac{\int_\Omega \boldsymbol{V}_p(\tau)\cdot\boldsymbol{V}_p(\tau)\,\mathrm{d}\Omega}{\int_\Omega \boldsymbol{V}_p(0)\cdot\boldsymbol{V}_p(0)\,\mathrm{d}\Omega}. \quad (7)$$

Here the adjoint evolution method outlined in Barkley *et al.* (2007) is employed, where the introduction of a state-transition operator $\mathcal{A} = e^{Lt}$, where L is a linear operator, allows for the time evolution of an arbitrary initial perturbation $\boldsymbol{V}_p$ to $t = \tau$ to be described by

$$\boldsymbol{V}_p(\tau) = \mathcal{A}(\tau)\boldsymbol{V}_p(0). \quad (8)$$

By further introducing an adjoint evolution operator $\mathcal{A}^*(\tau)$ of $\mathcal{A}$, that evolves an equivalent adjoint variable $\boldsymbol{V}_{p_\tau^*}$ backwards in time from $t = \tau$ to $t = 0$, (7) can be rewritten as

$$G(\tau) = \frac{\int_\Omega \boldsymbol{V}_p(0)\cdot\mathcal{A}^*(\tau)\mathcal{A}(\tau)\boldsymbol{V}_p(0)\,\mathrm{d}\Omega}{\int_\Omega \boldsymbol{V}_p(0)\cdot\boldsymbol{V}_p(0)\,\mathrm{d}\Omega}. \quad (9)$$

In this form, the optimal disturbance mode leading to $G(\tau)_{\max}$ is found through the determination of the leading eigenvalue and corresponding eigenvector of the operator $\mathcal{A}^*\mathcal{A}$. This optimal perturbation mode presents as the real and orthonormal right singular vector determined through the singular value decomposition of $\mathcal{A}^*\mathcal{A}$; which is solved using an implicitly restarted Arnoldi iterative method. The aim of the optimal linear growth portion of the present work can be formally written as

$$G(\tau)_{\max} = \max_{\boldsymbol{V}_p(0)} \frac{\int_\Omega \boldsymbol{V}_p(0)\cdot\mathcal{A}^*(\tau)\mathcal{A}(\tau)\boldsymbol{V}_p(0)\,\mathrm{d}V}{\int_\Omega \boldsymbol{V}_p(0)\cdot\boldsymbol{V}_p(0)\,\mathrm{d}V}. \quad (10)$$

The global maximum amplification $G_{\max}$ occurs at the optimal time interval τ_{opt} having streamwise wavenumber k_{opt}. From a physical perspective, $G_{\max}$ defines the global maximum growth in kinetic energy due to initial optimal linear conditions $\boldsymbol{V}_{p,\text{opt}}(0)$ evolved to time τ_{opt}. This is referred to as the optimal growth as it is the largest achievable gain in energy for all spatial wavenumbers k for a given Re and Ha dependent flow regime.

Numerical Methodology

A spatial high order nodal spectral element method incorporating a third-order time integration scheme based on backward-differencing is employed to discretise the governing equations and implement the transient growth analysis methodology. The domain is meshed using an average of 425 quadrilateral macro-elements with internally applied Langrangian polynomial shape functions defined as

$$L_i(\xi) = \prod_{g=1,g\neq i}^{N_p+1} \frac{\xi - \xi_g}{\xi_i - \xi_g}, \tag{11}$$

where ξ is the spatial coordinate, i and g the nodal indices, and N_p the polynomial order, which is varied to control spatial resolution in the spanwise x-y cross-plane. The nodal points within each element are spaced and weighted to correspond to Gauss-Legendre-Lobatto quadrature integration points, which reduce computational costs by forming diagonal mass matrices and leading to exponential spatial convergence. A graded element distribution was employed towards all solid surfaces to resolve regions that experience large flow gradients. The spacing of macro elements are scaled with respect to the Ha dependent boundary layer thickness; ensuring that a minimum of 8 macro elements span their height. Boundary conditions consist of zero velocities on all solid surfaces, a fully developed inlet velocity profile, along with high order pressure field Neumann boundary conditions on all domain perimeters to maintain third-order time accuracy (Karniadakis *et al.*, 1991).

A spectral-element-Fourier method analogous to the cylindrical formulation constructed in Blackburn and Sherwin (2004) is employed to capture three-dimensional flow variation in the streamwise z-direction. This method is well suited to simulation of flows where the geometry can be arbitrarily complex in a cross-plane but is infinite or periodic in an orthogonal direction (Karniadakis, 1990; Blackburn and Sherwin, 2004; Sheard *et al.*, 2009; Vo *et al.*, 2015). The velocity, pressure and electric potential fields are decomposed using this Fourier expansion in z with m streamwise modes such that

$$\begin{bmatrix} u(x,y,z,t) \\ v(x,y,z,t) \\ w(x,y,z,t) \\ p(x,y,z,t) \\ \phi(x,y,z,t) \end{bmatrix} = \sum_{j=0}^{m-1} \begin{bmatrix} u_m(x,y,t) \\ v_m(x,y,t) \\ w_m(x,y,t) \\ p_m(x,y,t) \\ \phi_m(x,y,t) \end{bmatrix} e^{ikmz} \tag{12}$$

where $k = 2\pi/L_z$ is the associated wavenumber in the z direction, and L_z is the periodicity length of the domain also in the z direction. The number of Fourier modes determines the spatial resolution in the orthogonal streamwise direction. The basic flow solution described by the fundamental Fourier mode was validated against the analytical solution for fully developed MHD flow as developed by Hunt and Stewartson (1965). For the transient growth analysis, the linearised equations require the construction of a single non-zero Fourier mode in the z-direction to completely define the eigenmodes as per (6). Streamwise wavenumbers are investigated between $0 \leq k \leq 80$, with the local maxima resolved to an accuracy of at least 0.1. To ensure that the optimal growths were captured sufficiently, and a monotonic decay in amplifications were achieved at higher τ, the analysis was conducted over time intervals extending to $\tau = 5\tau_{\text{opt}}$. Eigenvalue convergence of better than 0.01% was ensured for all the values presented in this paper. The linearised component of this solver has also been previously verified and implemented in works such as Hussam *et al.* (2012) and Tsai *et al.* (2016).

Local mesh refinement (h-refinement), shape function polynomial degree refinement (p-refinement) and Fourier mode refinement (where applicable) are used in ensuring grid independence and the convergence of the viscous drag coefficient C_{d} and the $\mathcal{L}^2$ norm. A polynomial order of $N_p = 8$ was deemed sufficient with a convergence of better than 0.3% achieved for all reference parameters. The minimum wavenumber (and in turn the maximum duct length L_z discretisation) required for the 3D simulations incorporating the non-linear MHD governing equations is given by the respective k of the optimal mode used to seed the base flow. For all but the highest initial perturbation energies ($10^{-6} \leq E_p \leq 10^{-3}$), 8 Fourier modes were found to be satisfactory for resolving the flow dynamics. For the highest perturbation case ($E_p = 10^{-2}$), 32 Fourier modes were required in congruence with an additional anti-aliasing method coming in the form of the two-thirds low-pass filtering technique outlined in Orszag (1971).

RESULTS AND DISCUSSION

Optimal Linear Transient Growth

The optimal modal gain in perturbation kinetic energy as a function of Hartmann number are presented and discussed in this section. The global maximum amplification $G_{\max}$ for $10 \leq Ha \leq 1000$ are provided in figure 2. Here, the results from Krasnov *et al.* (2010) and Pothérat (2007) are also shown for comparison. Transient growth was found to occur for all Ha present in this study, however, the magnitude of these amplifications is progressively suppressed with increasing Hartmann number. The monotonic reduction in energy growth is most likely due to the increased Joule dissipation found with higher magnetic field strengths. For $10 \leq Ha \leq 100$ the global maximum amplification is found in the present work to follow the trend $G_{\max} \approx 11.45 \times 10^3 Ha^{-1.6}$. This is in close agreement with the $G_{\max} \approx 8.8 \times 10^3 Ha^{-1.5}$ relationship obtained by the optimal growth analysis in Krasnov *et al.* (2010) over the limited range of $10 \leq Ha \leq 50$ as shown in figure 2. This also serves as further validation for the numerical framework used in this study.

For $150 \leq Ha \leq 1000$, the rate of change of $G_{\max}$ lessens with increasing Hartmann number. The scaling and growth rate predictions in this regime demonstrate a remarkable consistency with the SM82 model results from Pothérat (2007). For this higher Ha regime, the global maximum amplification recovers an approximate $-1/3$ power scaling of $G_{\max} \approx 25 \times 10^3 Ha^{-0.37}$. This is in stark contrast to the behaviour observed at lower field strengths $Ha \leq 150$, where there is a significant deviation between the scaling and energy gains predicted by both 3D and Q2D models. The mechanism producing maximum transient amplifications in low-Ha MHD flows and 3D Poiseuille flows result from the coupling of modes both invariant and variant in the vertical direction. These modes are the respective MHD equivalent of the well

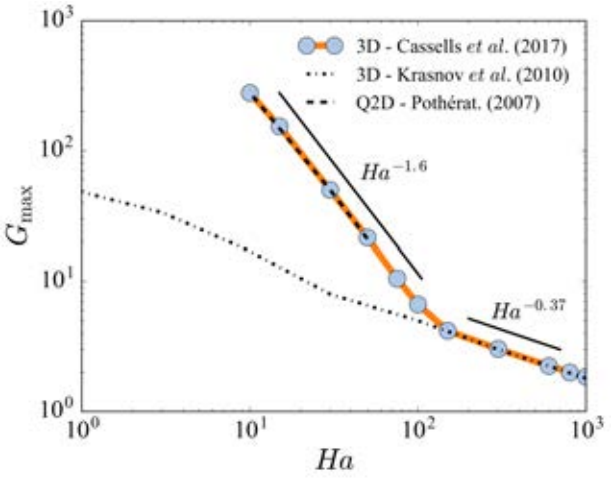

Figure 2: Global maximum amplifications as a function of Hartmann number. Here, pre-existing transient growth analysis data using a SM82 model (Pothérat, 2007) (dash-dotted line) and quasi-static MHD analysis (Krasnov *et al.*, 2010) (dashed line) are plotted for comparison against current results (orange line, grey markers).

known Orr–Sommerfeld and Squire modes found in hydrodynamic flows. Being of Q2D nature, the SM82 model can only combine the two-dimensional Orr–Sommerfeld equivalent modes for energy amplification. As the present findings show such strong alignment of the 3D duct optimal growths predictions for $150 \leq Ha \leq 1000$ with the SM82 model, this suggests that for adequately large field strengths (here $Ha \geq 150$), suppression of the streamwise invariant modes has occurred to allow the SM82 model to be an excellent predictor of optimal linear growth. Conversely, the coupling between streamwise variant and invariant modes plays a fundamental part in the enhancement of transient amplifications for $Ha \leq 150$; leading to the deviation between predicted growth rates at smaller Ha.

This explanation for the development of two well defined scaling regimes are further illustrated through a qualitative analysis of the perturbation field structures. The evolution of the eigenvector fields to time of maximum energy gain τ_{opt} for $Ha = 10, 100, 150$ and 600 are visualised via iso-surfaces of the spanwise component (x-z plane) of vorticity in figure 3. The perturbation fields for low to moderate Ha (figures 3 (a) and (b)) form complex overlapping homothetic structures within the sidewall layers. These streamwise aligned cigar-shaped modes are consistent with those producing maximum transient amplification in pure hydrodynamic flows (Pothérat, 2007). As Ha is increased in the first scaling regime $10 \leq Ha \leq 100$, the number of rolls in the vertical y direction also increase but maintain well defined periodicity. These disturbance modes also become increasingly flattened and localised within the thinning Shercliff layers in combination with a significant decrease in the optimal streamwise wavenumber.

In the second regime between $150 \leq Ha \leq 1000$, periodicity in y is lost, with a breakdown of the streamwise vortices occurring, as highlighted in figures 3(c,d). The flow becomes increasingly invariant in the magnetic field direction, such that by $Ha = 600$ only remnants of streamwise variation of vorticity remain, which are predominantly confined to the corner regions of the duct. The two-dimensionalisation of the optimal modes, and the relative invariance of the vorticity disturbance field in figures 3(c,d) 3(c,d), helps to illustrate the suspected diminishing influence of the Squire equivalent modes on the overall transient amplification of energy for $Ha \geq 150$. From a numerical methodology perspective this can have quite significant and meaningful implications. As Hartmann numbers in fusion reactor applications are typically quite large ($O(10^3)$), the ability of the SM82 model to accurately predict the dominant transient amplifications mechanisms at these larger field strengths allows for modelling to be conducted at significantly reduced computational costs. The reason being that the thin Hartmann layers do not require resolving when employing this Q2D model.

Nonlinear Temporal Evolution of Optimal Perturbations at High Hartmann Numbers

A three-dimensional basic flow seeded with optimal linear perturbations at varying initial energies for Ha = 600 and Re = 5000 will be analysed in this section. These flow regime parameters were chosen with a view towards representative magnetic field strengths seen in industrial applications (Smolentsev *et al.*, 2010). The energy of the perturbation field is given as a relative fraction of the unperturbed base flow energy, and defined using the ratio of volume integrals

$$E(t) = \frac{\int_\Omega \boldsymbol{V}_p \cdot \boldsymbol{V}_p \, \mathrm{d}\Omega}{\int_\Omega \boldsymbol{V}_0 \cdot \boldsymbol{V}_0 \, \mathrm{d}\Omega}. \tag{13}$$

The initial seeding energy of the optimal perturbation modes is defined as $E_p \equiv E(0)$, where $10^{-6} \leq E_p \leq 10^{-2}$ is presented here. The energy amplification of the perturbed flow can thus be measured using the temporal relation

$$G_n(t) = \frac{E(t)}{E_p}. \tag{14}$$

The energetic response due to the seeding of the base flow as a function of time is illustrated in figure 4. For the smallest initial seeding energy $E_p = 10^{-6}$, a very strong alignment with the temporal energy evolution modelled using the linearised governing equations is seen. As the seeding energy is increased, the magnitude of amplification is successively diminished in conjunction with a shortening of the time period at which the maximum occurs. For the maximum seeding energy $E_p = 10^{-2}$, no energy gain is observed for any time periods measured. For $E_p \leq 10^{-3}$, only single peaks in energy amplification are detected before a monotonic decay presents as $t \to \infty$. For a better understanding of the flow dynamics during these stages of transient growth, we introduce quantitative measures for viscous and magnetic dissipation, which are respectively defined as

$$\epsilon = 2\nu \sum_{\boldsymbol{k}} k^2 \left[\boldsymbol{V}(\boldsymbol{k}) \cdot \boldsymbol{V}(-\boldsymbol{k})\right], \tag{15}$$

$$\mu = \frac{\sigma}{\rho} \sum_{\boldsymbol{k}} \frac{(\boldsymbol{B_0} \cdot \boldsymbol{k})}{k^2} \left[\boldsymbol{V}(\boldsymbol{k}) \cdot \boldsymbol{V}(-\boldsymbol{k})\right]. \tag{16}$$

Here $\boldsymbol{k}$ is the wavenumber vector associated with a 3D Fourier decomposition. This is achieved through implementing a fast Fourier transform technique on discretely sampled data in the x-y plane in conjunction with a modal expansion using (12). The total viscous and magnetic dissipation normalised by their respective initial seeding energies are plotted as a function of time in figures 5 and 6, respectively. For $10^{-6} \leq E_p \leq 10^{-3}$, a significant increase in viscous dissipation is observed immediately after the base flow is seeded

(a) $Ha = 10$

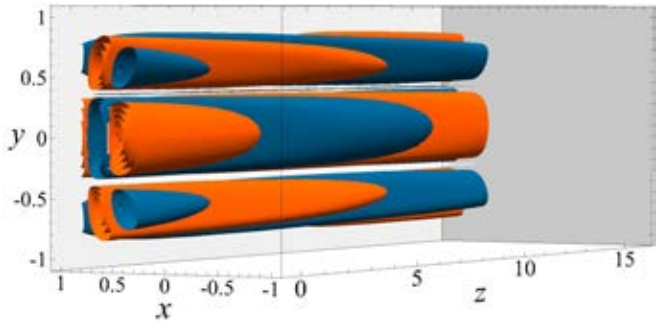

(b) $Ha = 100$

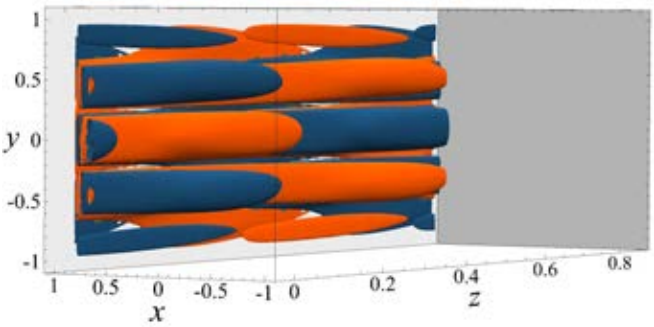

(c) $Ha = 150$

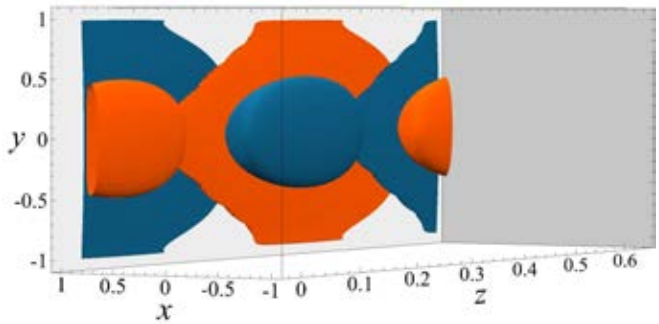

(d) $Ha = 600$

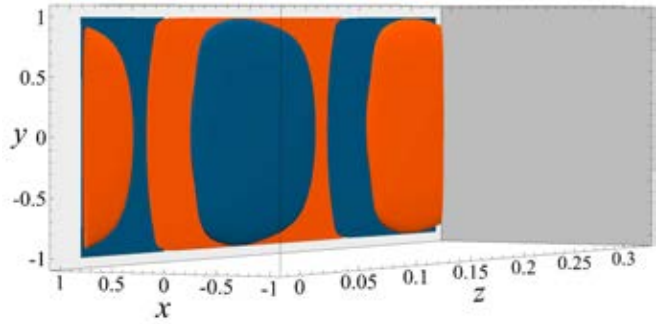

Figure 3: Vorticity iso-surfaces of the eigenvector fields producing the maximum transient amplification $G_{\max}$ evolved to τ_{opt} for $Ha = 10, 100, 150$ and 600 at $Re = 5000$. Blue and orange contours represent positive and negative spanwise vorticity, respectively. Contour levels are adjusted to approximately 90% of the maximum magnitude of vorticity. The flow is from left to right in the positive z-direction, with the magnetic field orientated vertically in the positive y-direction. For clarity, the vorticity is only plotted for $0 \leq x \leq 1$.

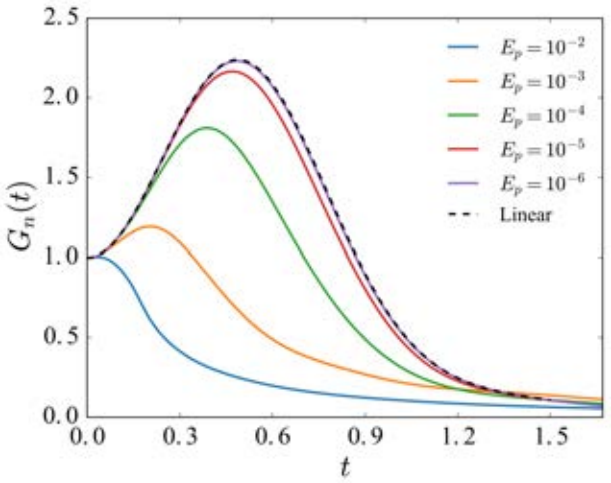

Figure 4: Temporal evolution of energy amplification due to seeding of the unperturbed base flow with the optimal disturbance mode corresponding to $Ha = 600$ at $Re = 5000$ for initial perturbation energies $10^{-6} \leq E_p \leq 10^{-2}$. Here the predicted growth rate using the linearised governing equations is also plotted (dashed line).

with the optimal mode. For $10^{-6} \leq E_p \leq 10^{-4}$, the peak in both magnetic dissipation and viscous dissipation appears to be strongly correlated with the corresponding time of maximum amplification seen in figure 4. For $E_p = 10^{-3}$ only the latter is strongly correlated, with no relationship seen for $E_p = 10^{-2}$. At $t \approx 0.2$, a sharp increase in ϵ and a corresponding decrease in μ is observed for the highest energy $E_p = 10^{-2}$ case. At this point in time, the ratio $\mu/\epsilon \approx 1.1$ indicates that viscous dissipation is contributing in almost equal measure to the total dissipation rates in the flow. However, magnetic dissipation remains the dominant energy loss mechanism for all E_p and t investigated here. After reaching their respective peaks in dissipation rates, both ϵ and μ are observed to decay (not necessarily monotonically) as $t \to \infty$.

It is interesting to note here that as the initial seeding energy approaches the infinitesimal limit described by the linearised equations, the time rate of change of both dissipation mechanisms converge. In other words, $\partial\epsilon/\partial t \approx \partial\mu/\partial t$ as $E_p \to 10^{-\infty}$. It also appears that as the initial seeding energy is increased, and the relative importance of nonlinear terms in the solution in turn grows, a weakening of magnetic dissipation and conversely strengthening of viscous dissipation is produced. A partial explanation for the difference is through the larger cascade of energy transfer to higher Fourier mode wavenumbers seen for greater seeding energies (not published here). Magnetic dissipation acts equally on all scales, whereas the dissipating effects of viscosity are more pronounced for higher k. Hence, nonlinearity is seen to promote transfer of energy to high wavenumbers, where viscous damping is dominant, rather than dissipating energy through Joule damping at larger scales.

For further quantification of the dominant flow structures leading to observed energy growth and dissipative trends, we introduce a flow anisotropy measure

$$\mathcal{G} = \frac{\mathcal{G}_1 + \mathcal{G}_2}{2}, \tag{17}$$

where $\mathcal{G}_1$ and $\mathcal{G}_2$ are calculated using the normalised mean-

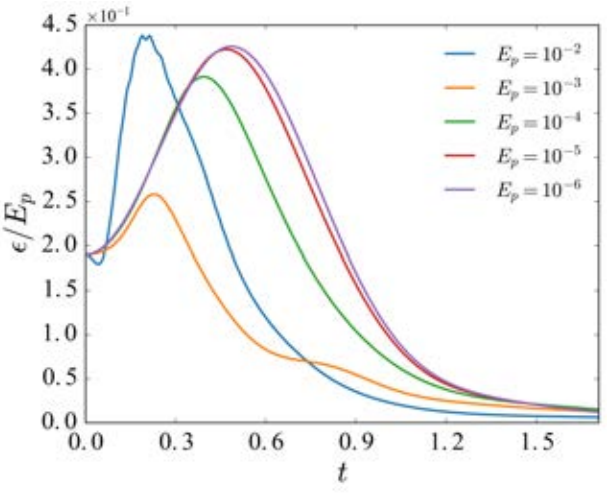

Figure 5: Temporal evolution of normalised viscous dissipation due to seeding of the unperturbed base flow with the optimal disturbance mode corresponding to $Ha = 600$ at $Re = 5000$ for initial perturbation energies $10^{-6} \leq E_p \leq 10^{-2}$.

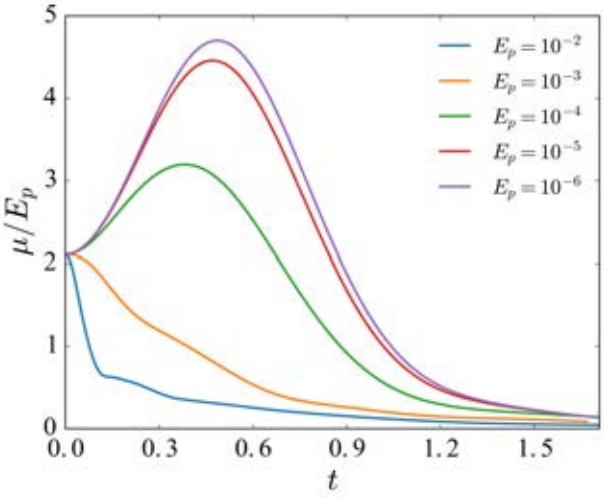

Figure 6: Temporal evolution of normalised magnetic dissipation due to seeding of the unperturbed base flow with the optimal disturbance mode corresponding to $Ha = 600$ at $Re = 5000$ for initial perturbation energies $10^{-6} \leq E_p \leq 10^{-2}$.

square velocity gradients

$$\mathcal{G}_1 = \frac{\langle(\partial u/\partial y)^2\rangle}{2\langle(\partial u/\partial x)^2\rangle} \quad \text{and} \quad \mathcal{G}_2 = \frac{2\langle(\partial \mathrm{v}/\partial \mathrm{y})^2\rangle}{\langle(\partial \mathrm{v}/\partial \mathrm{x})^2\rangle}. \qquad (18)$$

These anisotropy coefficients characterises the difference between the magnitudes of flow velocity derivatives taken along $(\partial/\partial y)$ and across $(\partial/\partial x)$ the magnetic field direction. They tend towards unity as a flow reaches a purely isotropic state, and towards zero in magnetic field direction independent anisotropic flow (Schumann, 1976). The primary cause for the changes in these derivatives are known to be due to the Joule dissipative effects found in MHD flows (Vorobev *et al.*, 2005). For 3D anisotropic flows, both coefficients in (18) tend towards one another. Hence, the average of the two, which are considered in (17), provide a good measure for the overall level of anisotropy in the flow.

The time history of (17) is plotted for varying optimal mode seeding energies in figure 7. Immediately onwards from $t = 0$, a rapid increase in $\mathcal{G}$ is observed for all E_p cases. Multiple peaks in flow isotropy are detected for all cases, where the initial peak occurs at a slightly delayed time interval in comparison to the time of maximum energy gain seen in figure 4. It is important to note that the measured decrease in flow anisotropy is small for all cases $\left(O(10^{-2}) - O(10^{-1})\right)$. The flow remains dominated by anisotropic structures, yet has small but finite intermittent bursts of relative isotropy. For $10^{-4} \leq E_p \leq 10^{-2}$ the secondary peaks in $\mathcal{G}$ are equal to or greater than the initial peak magnitude. In contrast, for lower seeding energies $E_p \leq 10^{-5}$, the degree of anisotropy increases after reaching a minimum at the first initial maxima seen in figure 7. It is interesting to note here that although Joule dissipation remains strong for all E_p, as seen in figure 6, this does not necessitate the temporal smoothing of the velocity field so that a monotonic trend towards a purely anisotropic state occurs. Exploiting this behaviour could pose as useful for future investigations into eliciting further transient growth and, potentially, instabilities.

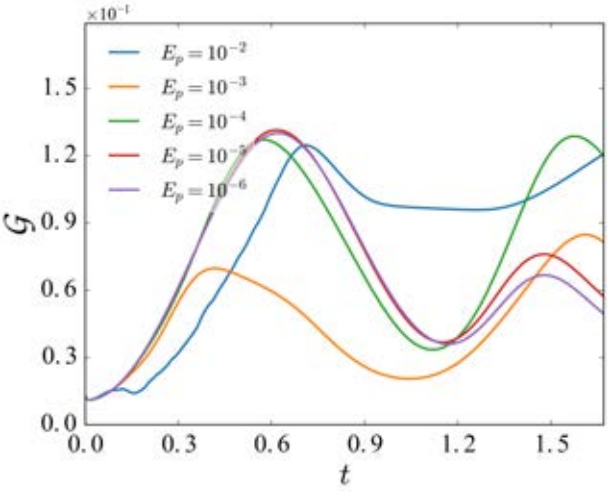

Figure 7: Temporal evolution of the degree of anisotropy due to seeding of the unperturbed base flow with the optimal disturbance mode corresponding to $Ha = 600$ at $Re = 5000$ for initial perturbation energies $10^{-6} \leq E_p \leq 10^{-2}$.

CONCLUSION

The global maximum transient amplifications of an electrically conducting fluid under the influence of a transverse magnetic field were investigated. A range of Hartmann numbers for $10 \leq Ha \leq 1000$ were studied at a fixed $Re = 5000$. It was shown that two regimes exists for scaling of maximum transient growth amplification; when perturbation structures are dominated by 3D modes a scaling of $G_{\max} \propto Ha^{-1.6}$ for $10 \leq Ha \leq 100$ was found, and $G_{\max} \propto Ha^{-0.37}$ in the range of $150 \leq Ha \leq 1000$ for when optimal disturbances become predominantly Q2D. Through comparison with existing literature, the SM82 model for Q2D MHD flow was found to be a valid predictor of optimal linear growths in this regime.

A subsequent investigation into seeding of an optimal mode corresponding to a high Ha regime into an unperturbed base flow to study the dynamic response was also conducted. At $Ha = 600$ and $Re = 5000$, it was determined that the initial energy of the perturbation modes plays a fundamental role in not only in the transient growth of energy, but also in the dominant dissipation and anisotropy forming mechanisms. No energy amplification above the linear prediction was ob-

served for any nonlinear case. As the seeding energy amplitude reduces in magnitude, it more closely recovers the linear growth predictions. Additionally, the time at which their respective maxima in energy occurs is closely correlated with the time of maximum dissipation. However, this time interval is increasingly shortened as the perturbation seeding energy magnitude grows. It was found that no growth occurs for $E_p = 10^{-2}$, which is in congruence with a sharp increase in viscous dissipation and combined decrease in magnetic dissipation. The likely reason being that as the initial energy is increased, and nonlinear terms in the solution become more significant, a greater transfer of energy to larger wavenumbers k tends to occur. Lastly, it was shown that the flow is dominated by anisotropy for all t and E_p, but experiences intermittent bursts of increased isotropy.

ACKNOWLEDGEMENTS

O. G. W. C. was supported by an Engineering Research Living Allowance (ERLA) scholarship from the Faculty of Engineering, Monash University. This research was supported by Discovery Grant DP150102920 from the Australian Research Council, and was undertaken with the assistance of resources from the National Computational Infrastructure (NCI), which is supported by the Australian Government.

REFERENCES

BARKLEY, D., BLACKBURN, H. and SHERWIN, S. (2007). "Direct optimal growth analysis for timesteppers". *Int. J. Numer. Methods Fluids*, **231**, 1–20.

BLACKBURN, H.M. and SHERWIN, S. (2004). "Formulation of a Galerkin spectral element–Fourier method for three-dimensional incompressible flows in cylindrical geometries". *Journal of Computational Physics*, **197(2)**, 759–778.

BOECK, T., KRASNOV, D., THESS, A. and ZIKANOV, O. (2008). "Large-scale intermittency of liquid-metal channel flow in a magnetic field". *Phys. Rev. Lett.*, **101(24)**, 244501.

CASSELLS, O.G.W., HUSSAM, W.K. and SHEARD, G.J. (2016). "Heat transfer enhancement using rectangular vortex promoters in confined quasi-two-dimensional magnetohydrodynamic flows". *Int. J. Heat Mass Transfer*, **93**, 186–199.

HAMID, A.H.A., HUSSAM, W.K. and SHEARD, G.J. (2016). "Combining an obstacle and electrically driven vortices to enhance heat transfer in a quasi-two-dimensional MHD duct flow". *J. Fluid Mech*, **792**, 364–396.

HAMID, A.H., HUSSAM, W.K., POTHÉRAT, A. and SHEARD, G.J. (2015). "Spatial evolution of a quasi-two-dimensional Kármán vortex street subjected to a strong uniform magnetic field". *Phys. Fluids*, **27(5)**, 053602.

HUNT, J.C.R. and STEWARTSON, K. (1965). "Magnetohydrodynamic flow in rectangular ducts. ii". *J. Fluid Mech.*, **23(3)**, 563–581.

HUSSAM, W.K., THOMPSON, M.C. and SHEARD, G.J. (2012). "Optimal transient disturbances behind a circular cylinder in a quasi-two-dimensional magnetohydrodynamic duct flow". *Phys. Fluids*, **24**, 024105.

KARNIADAKIS, G. (1990). "Spectral element-fourier methods for incompressible turbulent flows". *Computer Methods in Applied Mechanics and Engineering*, **80(1)**, 367–380.

KARNIADAKIS, G.E., ISRAELI, M. and ORSZAG, S.A. (1991). "High-order splitting methods for the incompressible Navier-Stokes equations". *Journal of computational physics*, **97(2)**, 414–443.

KRASNOV, D., ZIKANOV, O., ROSSI, M. and BOECK, T. (2010). "Optimal linear growth in magnetohydrodynamic duct flow". *J. Fluid Mech.*, **653(1)**, 273–299.

KRASNOV, D., ZIENICKE, E., ZIKANOV, O., BOECK, T. and THESS, A. (2004). "Numerical study of the instability of the Hartmann layer". *J. Fluid Mech.*, **504**, 183–211.

MORESCO, P. and ALBOUSSIERE, T. (2004). "Experimental study of the instability of the hartmann layer". *J. Fluid Mech*, **504**, 167–181.

NÁRAIGH, LENNON, O. (2015). "Global modes in nonlinear non-normal evolutionary models: Exact solutions, perturbation theory, direct numerical simulation, and chaos". *Physica D*, **309**, 20–36.

ORSZAG, S.A. (1971). "On the elimination of aliasing in finite-difference schemes by filtering high-wavenumber components". *Journal of the Atmospheric sciences*, **28(6)**, 1074–1074.

POTHÉRAT, A. (2007). "Quasi-two-dimensional perturbations in duct flows under transverse magnetic field". *Phys. Fluids*, **19**, 074104.

POTHÉRAT, A., SOMMERIA, J. and MOREAU, R. (2000). "An effective two-dimensional model for MHD flows with transverse magnetic field". *J. Fluid Mech*, **424**, 75–100.

SCHUMANN, U. (1976). "Numerical simulation of the transition from three- to two-dimensional turbulence under a uniform magnetic field". *J. Fluid Mech*, **74(01)**, 31–58.

SHEARD, G.J., FITZGERALD, M.J. and RYAN, K. (2009). "Cylinders with square cross-section: wake instabilities with incidence angle variation". *J. Fluid Mech*, **630**, 43–69.

SMOLENTSEV, S., VETCHA, N. and MOREAU, R. (2012). "Study of instabilities and transitions for a family of quasi-two-dimensional magnetohydrodynamic flows based on a parametrical model". *Phys. Fluids*, **24**, 024101.

SMOLENTSEV, S., WONG, C., MALANG, S., DAGHER, M. and ABDOU, M. (2010). "MHD considerations for the DCLL inboard blanket and access ducts". *Fus. Eng. Des.*, **85(7)**, 1007–1011.

SOMMERIA, J. (1988). "Electrically driven vortices in a strong magnetic field". *J. Fluid Mech.*, **189**, 553–569.

SOMMERIA, J. and MOREAU, R. (1982). "Why, how, and when, MHD turbulence becomes two-dimensional". *J. Fluid Mech.*, **118**, 507–518.

TAKASHIMA, M. (1996). "The stability of the modified plane poiseuille flow in the presence of a transverse magnetic field". *Fluid dynamics research*, **17(6)**, 293–310.

TSAI, T., HUSSAM, W.K., FOURAS, A. and SHEARD, G.J. (2016). "The origin of instability in enclosed horizontally driven convection". *Int. J. Heat Mass Transfer*, **94**, 509–515.

VO, T., MONTABONE, L., READ, P.L. and SHEARD, G.J. (2015). "Non-axisymmetric flows in a differential-disk rotating system". *J. Fluid Mech*, **775**, 349–386.

VOROBEV, A., ZIKANOV, O., DAVIDSON, P.A. and KNAEPEN, B. (2005). "Anisotropy of magnetohydrodynamic turbulence at low magnetic reynolds number". *Phys. Fluids*, **17(12)**, 125105.